Geophysical Research Letters

RESEARCH LETTER
10.1029/2019GL083647

# Observational Evidence of Horizontal Transport-Driven Dehydration in the TTL

**Laura L. Pan[1], Shown B. Honomichl[1], Troy Thornberry[2,3], Andrew Rollins[2], T. Paul Bui[4], Leonhard Pfister[4], and Eric E. Jensen[4]**

[1]National Center for Atmospheric Research, Boulder, CO, USA, [2]Chemical Sciences Division, NOAA Earth System Research Laboratory, Boulder, CO, USA, [3]Cooperative Institute for Research in Environmental Sciences, University of Colorado Boulder, Boulder, CO, USA, [4]NASA Ames Research Center, Moffett Field, Mountain View, CA, USA

**Key Points:**
- Airborne measurements over the western Pacific provide insight into the TTL hypothesis of horizontal transport-driven dehydration
- The observed final dehydration is dominated by quasi-horizontal transport between the lapse rate and the cold point tropopause
- The measured water vapor in the upper tropical tropopause layer corresponds to the coldest temperatures in the observation region

**Correspondence to:**
L. L. Pan,
liwen@ucar.edu

**Citation:**
Pan, L. L., Honomichl, S. B., Thornberry, T., Rollins, A., Bui, T. P., Pfister, L., & Jensen, E. E. (2019). Observational evidence of horizontal transport-driven dehydration in the TTL. *Geophysical Research Letters*, *46*, 7848–7856. https://doi.org/10.1029/2019GL083647

Received 8 MAY 2019
Accepted 27 JUN 2019
Accepted article online 1 JUL 2019
Published online 12 JUL 2019



**Abstract** A recent airborne study obtained extensive measurements in the tropical tropopause layer (TTL) over the western Pacific and provided the first opportunity to examine the relationship between water vapor and temperature in the coldest region and season of the TTL using high-resolution in situ data. Analysis of this data set verifies key hypotheses in Lagrangian simulations of TTL transport and freeze drying. Furthermore, the observations provide a number of new insights into the transport process: In the layer below the lapse rate tropopause, vertical transport from upward motion dominates the relative humidity structure; final dehydration, dominated by large-scale horizontal advection, occurs in the layer transacting the cold point tropopause that is often above the lapse rate tropopause, resulting in water vapor mixing ratios with corresponding frost points consistent with the coldest temperatures of the region, lower than the temperatures of the local cold points.

**Plain Language Summary** Stratospheric water vapor plays a significant role in the Earth's climate. Understanding the mechanisms regulating the amount of stratospheric water vapor is essential for predictions of future climate. Due to uncertainties in dehydration mechanisms, correctly simulating stratospheric water vapor is challenging for global climate models. Although a broad conceptual understanding of the atmospheric freeze-drying process was established by the mid-twentieth century, quantitative understanding of how transport and microphysics interact to control stratospheric water vapor is still limited. In situ measurements in the coldest region of the tropical tropopause layer made using the NASA Global Hawk unmanned aircraft present a significant data set for making new progress in this area of research.

## 1. Introduction

The conceptual framework of the tropical tropopause layer (TTL) was developed over a 10-year period starting around 2000, largely motivated by the challenge of understanding the mechanisms controlling stratospheric water vapor and its climate impact (de Forster & Shine, 2002; Dessler et al., 2013; Solomon et al., 2010). The core TTL concept as proposed by Hartmann et al. (2001) and Holton and Gettelman (2001) emphasizes the importance of horizontal transport in dehydrating the air mass that eventually enter the stratosphere. These works hypothesized that final dehydration of slowly rising TTL air was largely driven by horizontal cycling of air though the cold tropopause region over the tropical western Pacific (TWP). This process could explain why the observed lower stratospheric water vapor mixing ratio is significantly lower than that expected from the minimum temperature of the local tropopause. This hypothesis has since been quantitatively evaluated in a number of Lagrangian model analyses (Fueglistaler et al., 2004; Gettelman et al., 2002; Krüger et al., 2008; Rex et al., 2014; Schoeberl & Dessler, 2011). These modeling studies led to the concept of the Lagrangian Cold Point (LCP), the location at which air parcels encounter the minimum saturation mixing ratio (typically at the coldest temperature) along their path to the stratosphere. This series of studies also showed that the highest concentration and the coldest LCPs occur during boreal winter over the TWP. The LCP concept resolves the controversy surrounding the earlier "stratospheric fountain" hypothesis (Newell & Gould-Stewart, 1981), which suggested that transport of air into the stratosphere occurs preferentially over the TWP.

To verify this hypothesis observationally, in situ measurements from dedicated field campaigns are critical, since the existing satellite data do not have the necessary spatial resolution to resolve the dehydration

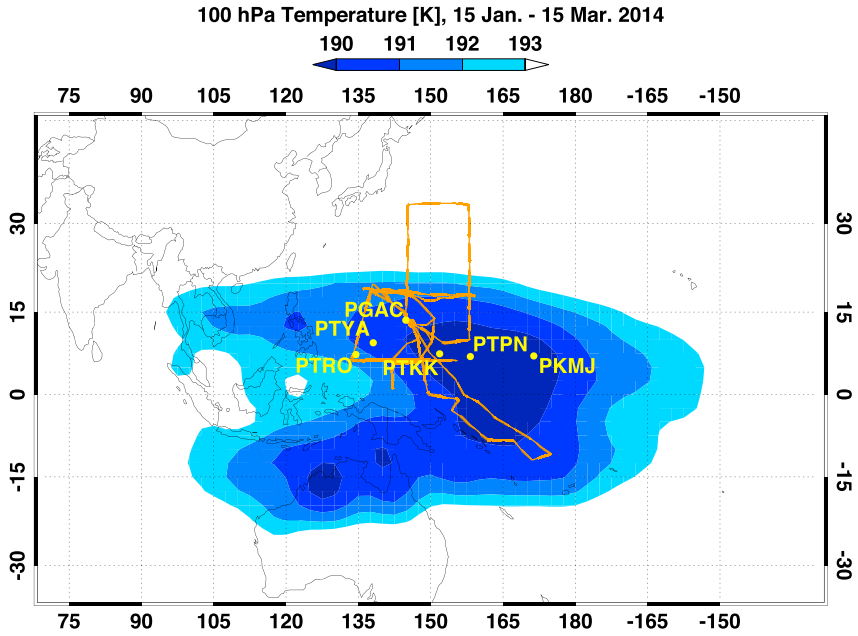


**Figure 1.** Global Hawk flight tracks for the six research flights during ATTREX 2014 and the mean 100-hPa temperature for the flight period (15 January to 15 March 2014) from NCEP/NCAR reanalysis data (Kalnay et al., 1996). The thickness of the lines for the flight tracks is inversely scaled by the pressure level of the flight, highlighting the nearly continuous vertical profiling between approximately 14.5 and 18.5 km as the key feature of the flight pattern. Locations of six regional National Weather Service stations are shown by yellow dots with station ID.

signature. Although a number of airborne field campaigns have targeted the TTL and dehydration mechanisms (MacKenzie et al., 2006; Schiller et al., 2009; Toon et al., 2010), it was not until 2014 that the first significant set of in situ measurements in the TTL over the TWP, the region of largest concentration of LCP, was obtained in the NASA Airborne Tropical Tropopause Experiment (ATTREX; Jensen, Pfister et al., 2017).

In this letter, we present an analysis of simultaneous high spatial resolution measurements of water vapor and temperature over the TWP from ATTREX. The main objective is to present observational evidence for the importance of horizontal transport-driven dehydration and the associated role of the LCP. This analysis is closely related to recent works on relative humidity distribution in the TTL (Jensen et al., 2017; Rollins et al., 2016; Schoeberl et al., 2019) and on lapse rate and cold point tropopause (CPT) definitions (Pan et al., 2018).

## 2. ATTREX Observations and Radiosondes

The NASA ATTREX 2014 deployment to the TWP (Eric J. Jensen et al., 2017) conducted six research flights, totaling ~100 flight hours, with the Global Hawk unmanned aircraft system from Guam (13.5°N, 144.8°E) during February and March. The analysis presented here uses mainly atmospheric state parameters, especially temperature data, measured by the Meteorological Measurement System (Scott et al., 1990), and water vapor ($H_2O$) data, measured by the NOAA-H2O two-channel, internal-path tunable diode laser hygrometer (Thornberry et al., 2015), both onboard the Global Hawk. These data are reported at 1 Hz, corresponding to typical horizontal and vertical scales of 160 and <20 m, respectively. The measurement uncertainty of the $H_2O$ is 6% ± 0.23 ppmv (Thornberry et al., 2015). Combined with the temperature and pressure uncertainties of ±0.3 K and ±0.5 hPa, the uncertainty of the derived relative humidity with respect to ice (RHi) for the range of measurements is less than 15%.

The meteorological conditions of the TTL over the TWP during the campaign period are described in detail in the ATTREX overview article, including the dynamical background of each flight (Jensen, Pfister et al., 2017). Figure 1 shows the flight tracks of the six ATTREX 2014 research flights, highlighting that the

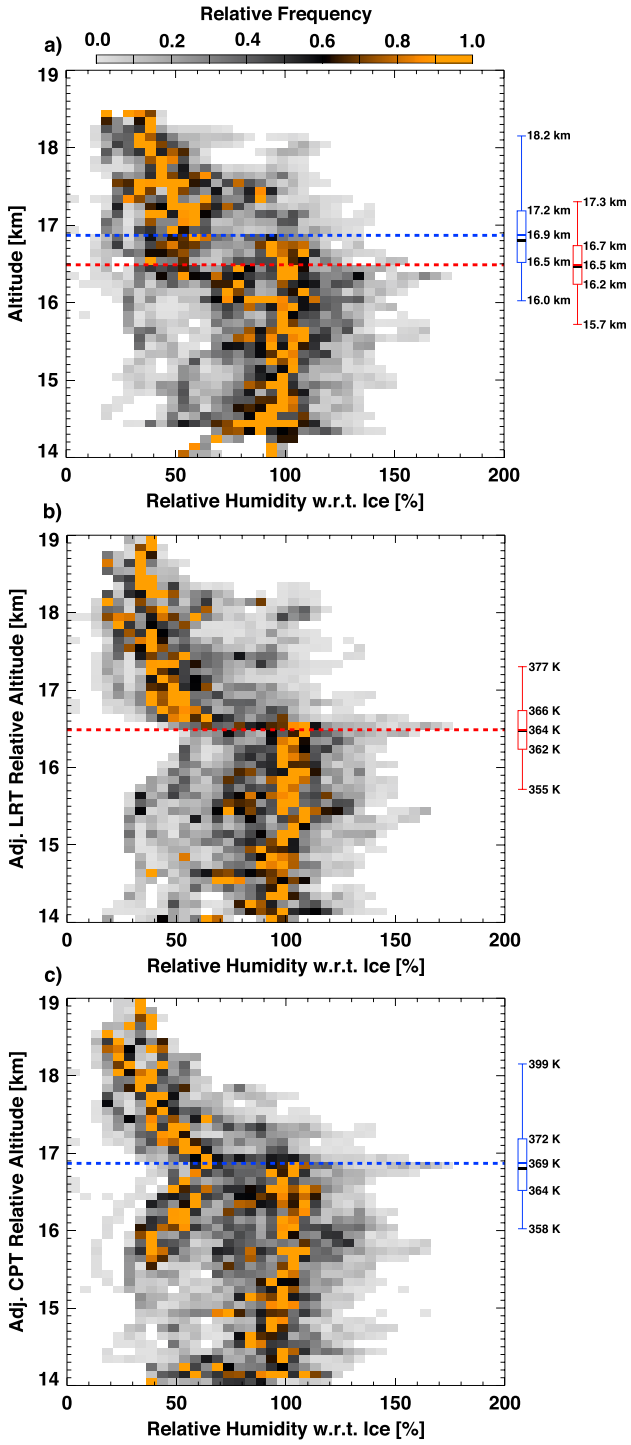


**Figure 2.** Layer-normalized relative frequency distributions of relative humidity with respect to ice in three vertical coordinates: (a) GPS altitude, (b) adjusted lapse rate tropopause (LRT) relative altitude, and (c) adjusted cold point tropopause (CPT) relative altitude. The average LRT and CPT heights from all profiles are shown as red and blue dashed lines, respectively. The bin size is 0.1 km vertically and 5% horizontally. To provide information on the height and distributions of the LRT and CPT, the minimum, maximum, and 25 and 75 percentiles are given by the box-and-whisker plots on the right side of each panel. The mean and the median in each case are given in blue and black ticks, respectively, in the box.

flights were conducted near the region of the coldest tropopause temperatures. Also shown in the figure are locations of six regional National Weather Service (NWS) stations, where radiosondes are launched twice daily at 0Z and 12Z. Radiosonde temperature profiles from these stations are provided in 100-m vertical resolutions and are used in the analysis to complement the airborne data.

## 3. Vertical and Horizontal Motion-Driven Dehydration Revealed by RHi in Tropopause Relative Coordinates

Physically, dehydration in the TTL is a freeze-drying process whereby ice crystals form and their growth and sedimentation remove water vapor in excess of ice saturation. The RHi of an air mass is controlled by coupled transport and microphysical processes. RHi can therefore be used as an effective tracer for the transport history of dehydration (Jensen, Thornberry, et al., 2017, and references therein). In this work, we focus on an analysis of RHi using tropopause relative coordinates, which serve to combine lapse rate information with RHi to diagnose the transport process driving dehydration. Both the lapse rate tropopause (LRT; World Meteorological Organization, 1957) and the CPT (Highwood & Hoskins, 1998) are used. Note that the analysis presented in Pan et al. (2018) demonstrated that the LRT is a better identifier of the tropical tropopause. The RHi analysis below provides further evidence for this conclusion.

Figure 2 shows the distribution of RHi derived from in situ data using all Global Hawk profiles within the region from 20°S to 20°N latitude range and 130°E to 180°E longitude range. The distributions are shown as layer-normalized relative frequency using three different vertical coordinates: GPS altitudes (Figure 2a), adjusted LRT relative altitudes (Figure 2b), and adjusted CPT relative altitudes (Figure 2c). The adjusted relative altitude coordinates, $Z_{ar}$, are defined by altitude relative to the tropopause and adjusted by the mean tropopause altitude, following equation (1):

$$Z_{ar} = \overline{Z_{TP}} + (Z - Z_{TP}), \quad (1)$$

where $Z$ is regular altitude, $Z_{TP}$ is the corresponding tropopause (LRT or CPT) altitude for the profile, and $\overline{Z_{TP}}$ is the average tropopause (Pan & Munchak, 2011). The layer-normalized relative frequency is calculated using the number of samples in each RHi bin divided by the number in the highest sampling bin in the same layer.

The RHi distributions in the three coordinates show broad ranges including supersaturation up to approximately 160%. A detailed analysis and quantification of supersaturation has been given in Rollins et al. (2016) and Jensen, Thornberry, et al. (2017). In this work, we focus on the *modal* profiles of the RHi distribution, that is, the vertical distribution of the layer maxima, which reveals the dominant relationship between saturation processes and the temperature structure.

Contrasting the modal profiles in three different coordinates, a number of features become apparent. Foremost, the modal profile in LRT relative altitude coordinate (Figure 2b) shows a strong discontinuity in the dehydration process at the tropopause. The approximately 100% RHi

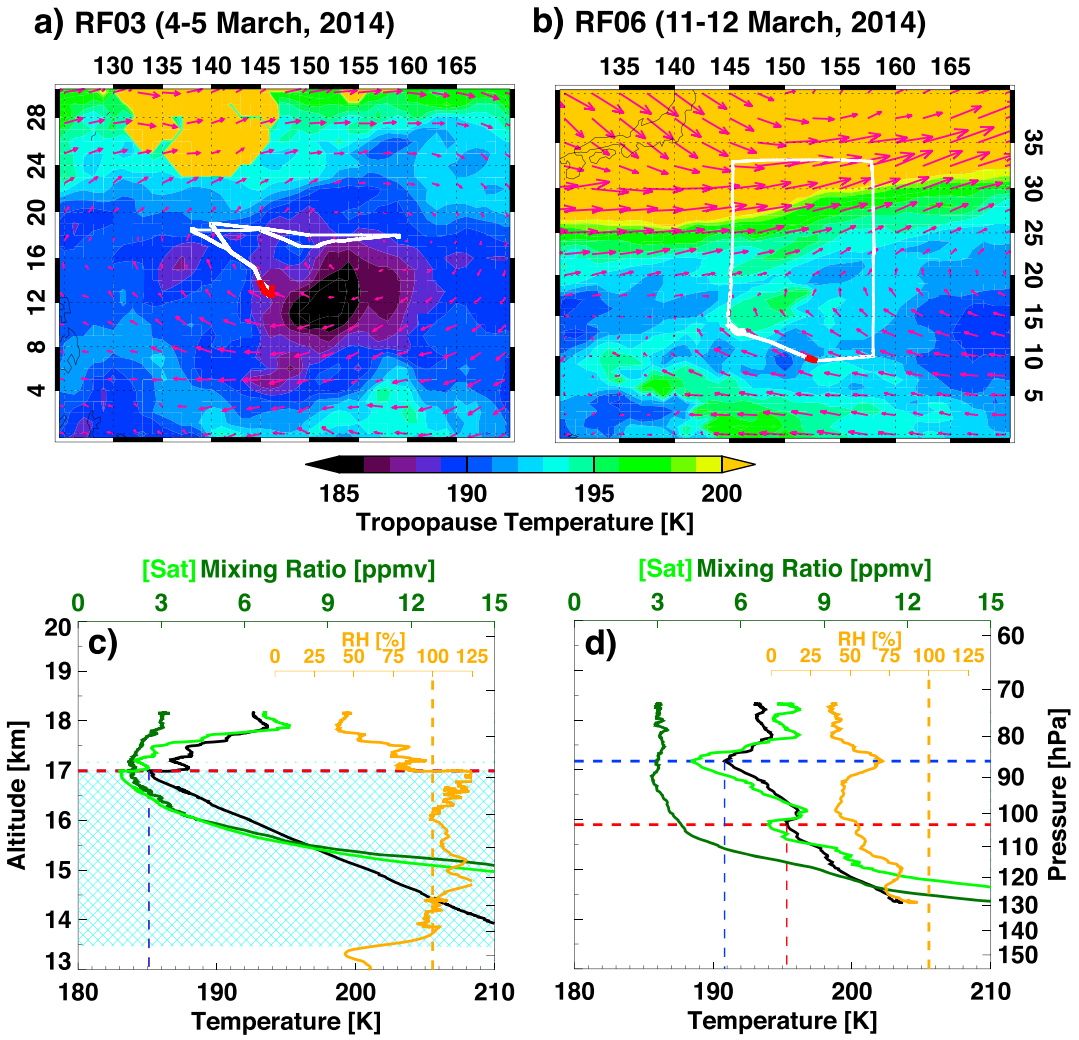


**Figure 3.** Two selected flights and profiles to provide examples for "local dehydration" and "upstream dehydration." (a) The flight track of RF03 (white line) and the tropopause level temperature (color shading) and wind fields (pink arrows). (b) Same as (a) but for RF06. (c) A selected profile from RF03. See the red segment in (a) for the profile's location. The four profiles shown are temperature (black), water vapor mixing ratio (dark green) from measurements, the saturation vapor mixing ratio (light green) derived from the temperature measurements, and derived relative humidity with respect to ice (orange). The light blue shading indicates the layer of in-cloud measurements. The lapse rate tropopause and cold point tropopause altitudes are marked by red and blue dashed lines, respectively. For this profile, they are colocated so only the red is seen. (d) Same as (c) but for a selected profile in RF06. The location of the profile is indicated in (b).

modal value between 14 km and the LRT indicates that upward vertical motion dominates the dehydration process below the LRT. The vertical motions attributed to diabatic and adiabatic processes have been analyzed using reanalysis data (Schoeberl et al., 2019). The relatively low altitude of the level of zero radiative heating and the anomalously strong positive heating over the wintertime western Pacific may also contribute to the prevalence of saturated air during the season (Jensen et al., 2015; Yang et al., 2010). Although the flights were planned to avoid convective activities so no immediate convective process was sampled during ATTREX flights, indirect convective influence is still possible from ubiquitous convection over the TWP during the season that left the saturated air behind.

The near 100% RHi mode also appears in the CPT relative coordinates (Figure 2c). There is, however, a bimodal structure in the 1.5 km below the CPT: a saturated mode (near 100% RHi) and a subsaturated mode (near 50% RHi). These two modes reveal distinct transport histories for the dehydration: While the saturated mode reflects the in situ dehydration process consistent with vertical motion driven dehydration, the subsaturated mode reflects nonlocal dehydration, in which the humidity in these air masses

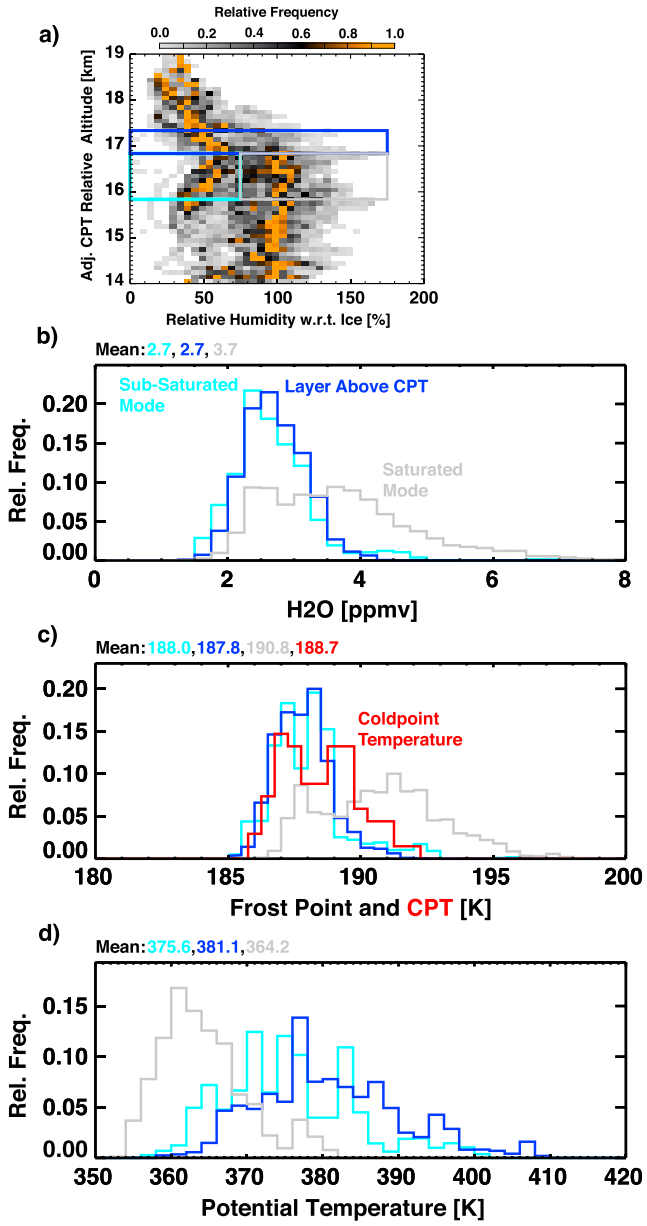


**Figure 4.** Histograms of (b) water vapor mixing ratio, (c) dewpoint temperature, and (d) potential temperature for three groups of measurements, with color coding (blue, cyan, and gray) that matches the selection boxes in (a). The three groups are selected to represent the layer above the cold point tropopause (CPT; depth = 0.5 km, blue), the layer below the CPT (depth = 1 km) with relative humidity with respect to ice < 75% (cyan) and relative humidity with respect to ice > 75% (gray). The additional histogram (red) in (c) is the distribution of CPT temperature from in situ profile measurements.

is a result of quasi-horizontal transport-driven dehydration, where the transported air masses encountered colder temperatures upstream. Furthermore, the contrast between the two relative coordinate distributions indicates that these subsaturated air masses were largely observed in the group of samples between the LRT and CPT.

To help understand these two modes of dehydration, we provide two sample profiles in Figure 3. Figures 3a and 3c show an example of local, or in situ, dehydration. In this profile, the LRT and CPT are collocated. The water vapor profile closely tracks the saturation vapor profile, derived using temperature measurement, below the tropopause. The figure also indicates that a thick layer of cloud was present below the tropopause, where the RHi was near 100%. The second example profile (Figures 3b and 3d) shows a case of upstream dehydration. Here the LRT and CPT are separated by more than a kilometer in altitude. The measured water vapor profile does not exhibit a relationship with the temperature profile, that is, it does not have a minimum at either the LRT or the CPT. The entire profile is cloud free and significantly subsaturated.

It is apparent from the tropopause level temperature and wind maps (Figures 3a and 3b) that these two profiles were sampled under very different large-scale background conditions. The first case was near the region of extremely low tropopause temperature (~185 K), and the second profile was sampled in a relatively warm background that is downstream from a colder region.

To quantify the importance of horizontal transport-driven dehydration and the role of the LCP, we examine the relationship between the samples above the CPT and the two modes in the samples below the CPT (Figure 2c) for three key variables: $H_2O$, the corresponding frost point temperature ($T_f$), and the potential temperature ($\theta$). The three subsets of data are plotted in Figures 4b–4d as indicated by the three boxes in Figure 4a. The blue box selects a 0.5-km depth layer above the CPT, the cyan box selects the subsaturated mode of data in the 1-km layer below the CPT, and the gray box selects the saturated mode in the same relative coordinate layer. The two modes are separated at 75% RHi.

The most significant message revealed by Figure 4 is that the subsaturated mode (cyan) below the CPT and the single mode in the samples above the CPT (blue) share similar distributions in all three variables: They have characteristically identical $H_2O$ and $T_f$, which should be recognized as resulting from upstream LCPs, and are also sampled within similar range of $\theta$. Note the distribution of sampled CPT temperatures is included in Figure 4c to show that the local CPT temperature for these data is on average 1 K warmer than the LCP. This comparison demonstrates that final dehydration is not controlled by the local CPT but by a significantly colder group of LCPs. A loose comparison with the average temperature map for the period (Figure 1) indicates that the distribution of $T_f$ (LCPs) from the two low $H_2O$ groups in Figure 4b corresponds to the average temperature of the center of the cold trap region, where $T$ < 190 K, although the daily locations of the coldest region varied during the campaign period (Jensen, Pfister, et al., 2017).

For the saturated mode (Figure 4, gray), although its $H_2O$ and $T_f$ distributions have a significant overlap with the other two groups, the distributions of both variables extend to higher values. Its average $H_2O$ and $T_f$ are 1 ppmv and 3 K higher. Its $\theta$ distribution is also very different from the other two groups and extends to significantly lower values, indicative of the air masses' tropospheric characteristics.

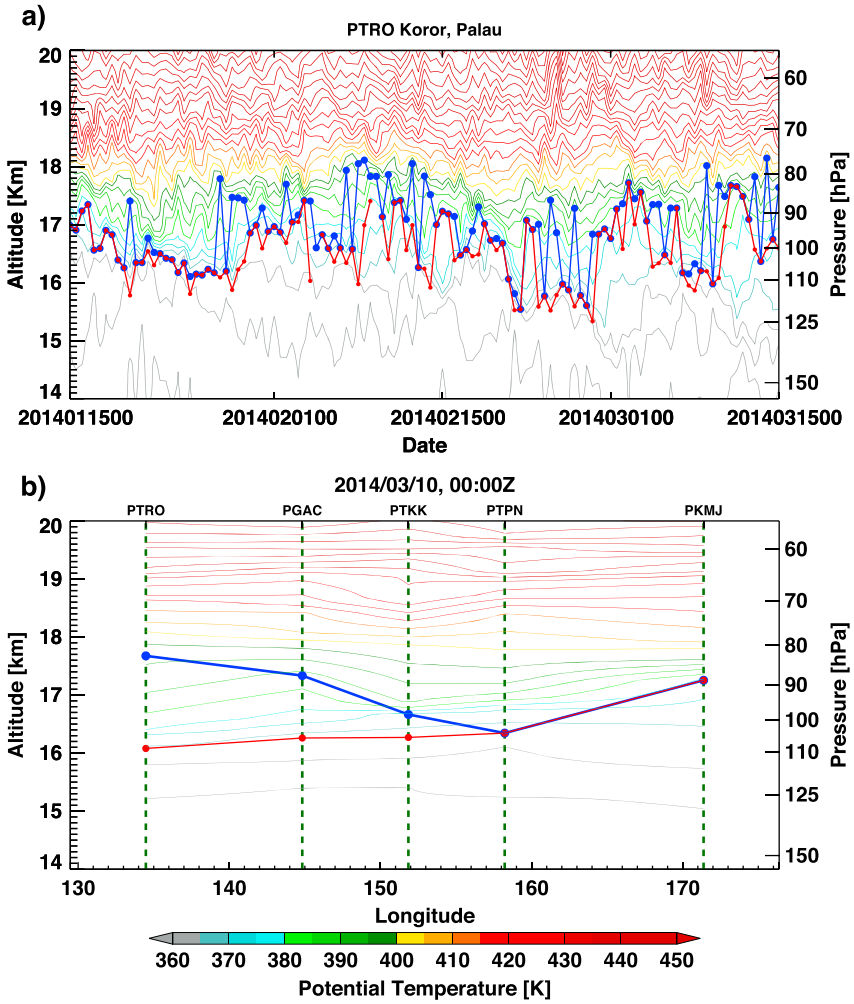


**Figure 5.** Isentropic structures and lapse rate tropopause and cold point tropopause heights derived from the National Weather Service temperature soundings. (a) Time-height cross section of $\theta$ created by twice-daily sounding data from PTRO (Koror Palau) for 1 Febuary to 15 March 2014. (b) Longitude-height cross section of $\theta$ derived from five regional National Weather Service stations data for a selected time (10 March 2014, 0Z). Contours represent 5-K intervals. Also shown are the lapse rate tropopause (red) and cold point tropopause (blue) derived from each profile.

It is interesting to note that although the two groups of measurements, subsaturated (cyan) and saturated (gray), appear to have the same altitude range relative to the CPT, they represent distinct air masses. On the other hand, the subsaturated group (cyan) and the group above the CPT (blue), although appearing on different sides of the local CPTs, are in effect the same air masses, the air masses of minimum $H_2O$ in the measurements.

## 4. Roles of Tropical Waves in Horizontal Transport-Driven Dehydration

The significant role of tropical waves in the dehydration process through the CPT temperature perturbation they generate and cirrus cloud formation they induce near the tropopause is a new component of dehydration research in the recent decade (e.g., Kim et al., 2016; Kim & Alexander, 2015; Podglajen et al., 2017, and references therein). In this section, we discuss the role of wave perturbations in connection with horizontal transport-driven dehydration. This discussion will also provide an explanation to part of the Figure 4 results, where the subsaturated samples below the CPT and the samples above the CPT appear to have similar characteristics.

Figure 5 illustrates the isentropic structure of the region and its relationship to the LRT and CPT, using the regional NWS sounding data, for selected cross sections. The TWP region is under the influence of various

types of tropical waves during the experiment (Jensen, Pfister, et al., 2017; Kim et al., 2016). The day-to-day variation is apparent in the time-height cross section of $\theta$ from the PTRO station temperature soundings (Figure 5a). The LRT and CPT from each sounding profile are plotted to indicate that the day-to-day variation of the LRT/CPT spans ~2 km in altitude (~16–18 km) and 30-K potential temperature range (~370–400 K). Despite the rapid vertical displacement, the LRT consistently marks the transition between layers of low static stability and high static stability, indicated by the sharp change in the vertical gradient of $\theta$ (plotted at 5-K intervals), which meets the expectation for a successful tropopause definition. The increased static stability above the LRT (indicated by larger gradient of θ) is also a direct indicator that horizontal, quasi-adiabatic advection begins to dominate the transport above this level.

An approximate longitude-height cross section of $\theta$ for a selected synoptic time (0Z 10 March) is constructed using soundings from five NWS stations (Figure 5b) to highlight the "sloping isentropes" that intersect the center of the coldest layer, marked by the CPT. This snap shot makes it apparent that air masses advected quasi-isentropically may encounter multiple CPTs, and only the coldest one sets the ultimate dehydration. This figure explains the conclusion drawn from Figure 4 that the layer sampled above the CPT and the non-local dehydration mode sampled below the CPT are in effect the same layer (~370–400 K), since their $T_f$ share the same distribution. This layer of minimum $H_2O$ straddles the CPTs because the tropical waves distribute the CPTs vertically within this layer.

## 5. Conclusions and Discussions

We have analyzed ATTREX in situ $H_2O$ and temperature data to directly verify the core hypothesis of dehydration in the TTL. The ATTREX observations verify the hypothesis that horizontal transport above the top of convection is the key determiner of final dehydration. The analysis provides an observed signature of LCP, a Lagrangian model-defined concept.

Using LRT- and CPT-relative coordinates, we arrive at a number of conclusions. Specifically,

1. RHi distributions in LRT- and CPT-relative coordinates show that vertical motion dominates the dehydration process below the LRT. The final dehydration, as diagnosed by the layer of lowest $H_2O$, however, is dominated by horizontal transport processes during the slow ascent across the layer around the coldest point, occurring mostly above the LRT in the 370- to 400-K $\theta$ layer.
2. The distribution of the frost point temperature for the measured minimum water vapor layer has a mean value lower than that corresponding to the measured local cold point temperatures, indicating that it is distinct from the in situ dehydration frost point and consistent with the center of the cold trap, the region of the seasonally averaged coldest tropopause layer temperature (<190 K). This result verifies the key role of the LCP, concentrated in the TWP cold trap, in controlling the lower stratospheric water vapor in the NH winter.
3. The RHi distribution shows that the stratospheric and tropospheric dynamic behavior (vertical- vs. horizontal-mixing dominated) is separated by the LRT. The final dehydration is therefore completed in the lower stratosphere as the boundary between stratosphere and troposphere is defined by the LRT.
4. This analysis also provides a different perspective on the importance of tropical waves in dehydration. As part of the temperature perturbation, the tropical waves induce vertical fluctuations of the isentropes and redistribute their relationship with the cold points, which in part facilitates the role of LCPs.

Since satellite observations lack the vertical resolution in the TTL to resolve the water vapor- temperature relationship in this thin layer and the ATTREX is the first large-scale airborne campaign in the region, the results described in this letter are the first direct observational evidence for the horizontal transport-driven dehydration hypothesis. These quantitative results, however, are still limited by the duration and spatial coverage of the campaign. Similar airborne studies are needed to investigate the dehydration process in the boreal summer season, when mixing from the extratropics and monsoon circulations play a larger role. Planned TTL measurements using long duration balloons (Haase et al, 2018) will present another opportunity to quantitatively investigate the global and seasonal behavior of dehydration processes that regulate stratospheric water vapor.

**Acknowledgments**

The flight data, including temperature and water vapor measurements used in this study, are available from NASA Earth Science Project Office website (espoarchive.nasa.gov). The NWS data are obtained from the Earth Systems Research Laboratory NWS radiosonde archive (https://esrl.noaa.gov/raobs/). NCEP/NCAR reanalysis output are provided by the NOAA/OAR/ESRL/PSD (https://www.esrl.noaa.gov/psd/).

## References

Dessler, A. E., Schoeberl, M. R., Wang, T., Davis, S. M., & Rosenlof, K. H. (2013). Stratospheric water vapor feedback. *Proceedings of the National Academy of Sciences*, *110*(45), 18,087–18,091. https://doi.org/10.1073/pnas.1310344110

de Forster, P. M., & Shine, K. P. (2002). Assessing the climate impact of trends in stratospheric water vapor. *Geophysical Research Letters*, *29*(6), 1086. https://doi.org/10.1029/2001GL013909

Fueglistaler, S., Wernli, H., & Peter, T. (2004). Tropical troposphere-to-stratosphere transport inferred from trajectory calculations. *Journal of Geophysical Research*, *109*, D03108. https://doi.org/10.1029/2003JD004069

Gettelman, A., Randel, W. J., Wu, F., & Massie, S. T. (2002). Transport of water vapor in the tropical tropopause layer. *Geophysical Research Letters*, *29*(1), 1009. https://doi.org/10.1029/2001GL013818

Haase, J. S., Alexander, M. J., Hertzog, A., Kalnajs, L., Deshler, T., Davis, S. M., et al. (2018). Around the world in 84 days. *Eos*, *99*. https://doi.org/10.1029/2018EO091907

Hartmann, D. L., Holton, J. R., & Fu, Q. (2001). The heat balance of the tropical tropopause, cirrus, and stratospheric dehydration. *Geophysical Research Letters*, *28*(10), 1969–1972. https://doi.org/10.1029/2000GL012833

Highwood, E. J., & Hoskins, B. J. (1998). The tropical tropopause. *Quarterly Journal of the Royal Meteorological Society*, *124*(549), 1579–1604. https://doi.org/10.1002/qj.49712454911

Holton, J. R., & Gettelman, A. (2001). Horizontal transport and the dehydration of the stratosphere. *Geophysical Research Letters*, *28*(14), 2799–2802. https://doi.org/10.1029/2001GL013148

Jensen, E. J., Pfister, L., Jordan, D. E., Bui, T. V., Ueyama, R., Singh, H. B., et al. (2017). The NASA Airborne Tropical Tropopause Experiment: High-altitude aircraft measurements in the tropical western pacific. *Bulletin of the American Meteorological Society*, *98*(1), 129–143. https://doi.org/10.1175/BAMS-D-14-00263.1

Jensen, E. J., Pfister, L., Ueyama, R., Bergman, J. W., & Kinnison, D. (2015). Investigation of the transport processes controlling the geographic distribution of carbon monoxide at the tropical tropopause. *Journal of Geophysical Research: Atmospheres*, *120*, 2067–2086. https://doi.org/10.1002/2014JD022661

Jensen, E. J., Thornberry, T. D., Rollins, A. W., Ueyama, R., Pfister, L., Bui, T., et al. (2017). Physical processes controlling the spatial distributions of relative humidity in the tropical tropopause layer over the Pacific. *Journal of Geophysical Research: Atmospheres*, *122*, 6094–6107. https://doi.org/10.1002/2017JD026632

Kalnay, E., Kanamitsu, M., Kistler, R., Collins, W., Deaven, D., Gandin, L., et al. (1996). The NCEP NCAR 40-Year Reanalysis Project. *Bulletin of the American Meteorological Society*, *77*(3), 437–471. Retrieved from https://journals.ametsoc.org/doi/pdf/10.1175/1520-0477%281996%29077%3C0437%3ATNYRP%3E2.0.CO%3B2

Kim, J., & Alexander, M. J. (2015). Tropopause temperature. *Geophysical Research Letters*, *42*, 1584–1592. https://doi.org/10.1002/2014GL062737

Kim, J.-E., Alexander, M. J., Bui, T. P., Dean-Day, J. M., Lawson, R. P., Woods, S., et al. (2016). Ubiquitous influence of waves on tropical high cirrus clouds. *Geophysical Research Letters*, *43*, 5895–5901. https://doi.org/10.1002/2016GL069293

Krüger, K., Tegtmeier, S., & Rex, M. (2008). Long-term climatology of air mass transport through the tropical tropopause layer (TTL) during NH winter. *Atmospheric Chemistry and Physics*, *8*(4), 813–823. https://doi.org/10.5194/acp-8-813-2008

MacKenzie, A. R., Schiller, C., Peter, T., Adriani, A., Beuermann, J., Bujok, O., et al. (2006). Tropopause and hygropause variability over the equatorial Indian Ocean during February and March 1999. *Journal of Geophysical Research*, *111*, D18112. https://doi.org/10.1029/2005JD006639

Newell, R. E., & Gould-Stewart, S. (1981). A stratospheric fountain? *Journal of the Atmospheric Sciences*, *38*(12), 2789–2796. https://doi.org/10.1175/1520-0469(1981)038<2789:asf>2.0.co;2

Pan, L. L., Honomichl, S. B., Bui, T. V., Thornberry, T., Rollins, A., Hintsa, E., & Jensen, E. J. (2018). Lapse rate or cold point: The tropical tropopause identified by in situ trace gas measurements. *Geophysical Research Letters*, *45*, 10,756–10,763. https://doi.org/10.1029/2018GL079573

Pan, L. L., & Munchak, L. A. (2011). Relationship of cloud top to the tropopause and jet structure from CALIPSO data. *Journal of Geophysical Research*, *116*, D12201. https://doi.org/10.1029/2010JD015462

Podglajen, A., Bui, T. P., Dean-Day, J. M., Pfister, L., Jensen, E. J., Alexander, M. J., et al. (2017). Small-scale wind fluctuations in the tropical tropopause layer from aircraft measurements: Occurrence, nature, and impact on vertical mixing. *Journal of the Atmospheric Sciences*, *74*(11), 3847–3869. https://doi.org/10.1175/jas-d-17-0010.1

Rex, M., Wohltmann, I., Ridder, T., Lehmann, R., Rosenlof, K., Wennberg, P., et al. (2014). A tropical West Pacific OH minimum and implications for stratospheric composition. *Atmospheric Chemistry and Physics*, *14*(9), 4827–4841. https://doi.org/10.5194/acp-14-4827-2014

Rollins, A. W., Thornberry, T. D., Gao, R. S., Woods, S., Lawson, R. P., Bui, T. P., et al. (2016). Observational constraints on the efficiency of dehydration mechanisms in the tropical tropopause layer. *Geophysical Research Letters*, *43*, 2912–2918. https://doi.org/10.1002/2016GL067972

Schiller, C., Groob, J. U., Konopka, P., Plöger, F., Silva Dos Santos, F. H., & Spelten, N. (2009). Hydration and dehydration at the tropical tropopause. *Atmospheric Chemistry and Physics*, *9*(24), 9647–9660. https://doi.org/10.5194/acp-9-9647-2009

Schoeberl, M. R., & Dessler, A. E. (2011). Dehydration of the stratosphere. *Atmospheric Chemistry and Physics*, *11*(16), 8433–8446. https://doi.org/10.5194/acp-11-8433-2011

Schoeberl, M. R., Jensen, E. J., Pfister, L., Ueyama, R., Wang, T., Selkirk, H., et al. (2019). Water vapor, clouds, and saturation in the tropical tropopause layer. *Journal of Geophysical Research: Atmospheres*, *124*, 3984–4003. https://doi.org/10.1029/2018JD029849

Scott, S. G., Bui, T. P., Chan, K. R., & Bowen, S. W. (1990). The meteorological measurement system on the NASA ER-2 aircraft. *Journal of Atmospheric & Oceanic Technology*, *7*(4), 525–540. https://doi.org/10.1175/1520-0426(1990)007<0525:TMMSOT>2.0.CO;2

Solomon, S., Rosenlof, K. H., Portmann, R. W., Daniel, J. S., Davis, S. M., Sanford, T. J., & Plattner, G. K. (2010). Contributions of stratospheric water rate of global warming. *Science*, *327*(5970), 1219–1223. https://doi.org/10.1126/science.1182488

Thornberry, T. D., Rollins, A. W., Gao, R. S., Watts, L. A., Ciciora, S. J., McLaughlin, R. J., & Fahey, D. W. (2015). A two-channel, tunable diode laser-based hygrometer for measurement of water vapor and cirrus cloud ice water content in the upper troposphere and lower stratosphere. *Atmospheric Measurement Techniques*, *8*(1), 211–224. https://doi.org/10.5194/amt-8-211-2015

Toon, O. B., Starr, D. O., Jensen, E. J., Newman, P. A., Platnick, S., Schoeberl, M. R., et al. (2010). Planning, implementation, and first results of the Tropical Composition, Cloud and Climate Coupling Experiment (TC4). *Journal of Geophysical Research*, *115*, D00J04. https://doi.org/10.1029/2009JD013073

WMO (World Meteorological Organization) (1957). Meteorological at all modern meteorological stations the precision instruments of. *WMO Bulletin*, *5*(4).

Yang, Q., Fu, Q., & Hu, Y. (2010). Radiative impacts of clouds in the tropical tropopause layer. *Journal of Geophysical Research*, *115*, D00H12. https://doi.org/10.1029/2009JD012393